Environmental Science: Atmospheres

ROYAL SOCIETY OF CHEMISTRY

PAPER

View Article Online
View Journal | View Issue

Cite this: *Environ. Sci.: Atmos.*, 2024, **4**, 88

The effect of temperature and relative humidity on secondary organic aerosol formation from ozonolysis of Δ^3-carene†

Ditte Thomsen, ‡[a] Emil Mark Iversen, ‡[a] Jane Tygesen Skønager, [a] Yuanyuan Luo,[b] Linjie Li,[c] Pontus Roldin,[df] Michael Priestley, [cg] Henrik B. Pedersen, [e] Mattias Hallquist, [c] Mikael Ehn,[b] Merete Bilde *[a] and Marianne Glasius *[a]

This study investigates the effects of temperature and relative humidity (RH) on the formation of secondary organic aerosol (SOA) from Δ^3-carene, a prevalent monoterpene in boreal forests. Dark ozonolysis experiments of 10 ppb Δ^3-carene were conducted in the Aarhus University Research on Aerosol (AURA) atmospheric simulation chamber at temperatures of 0, 10, and 20 °C. Under dry conditions (RH < 2%), the SOA formation in terms of both particle number and mass concentration shows minimal temperature dependence. This is in contrast to previous findings at higher initial concentrations and suggests an effect of VOC loading for Δ^3-carene. Interestingly, the mass fraction of key oxidation products (*cis*-3-caric acid, *cis*-3-caronic acid) exhibit a temperature dependence suggesting continuous condensation at lower temperatures, while evaporation and further reactions over time become more favourable at higher temperatures. The oxygen-to-carbon ratios in the particle phase and the occurrence of highly oxygenated organic molecules (HOM) in the gas phase show modest increases with higher temperatures. Predictions from the Aerosol Dynamics and Gas- and Particle-Phase Chemistry Kinetic Multilayer Model (ADCHAM) agrees with the experimental results regarding both physical particle properties and aerosol composition considering the experimental uncertainties. At high RH (~80%, 10 °C), a considerable increase in the particle nucleation rate and particle number concentration is observed compared to experiments under dry conditions. This is likely due to enhanced particle nucleation resulting from more stable cluster formation of water and inorganics at increased RH. However, RH does not affect the particle mass concentration.

Received 24th August 2023
Accepted 22nd November 2023

DOI: 10.1039/d3ea00128h

rsc.li/esatmospheres

Environmental significance

Atmospheric aerosols are known to affect both human health and climate, but the extent of their effects remains a large uncertainty in models of current and future climate. One such uncertainty lies in the limited understanding of the effect of temperature and relative humidity on the formation of secondary organic aerosol (SOA). In this work, we elucidate how temperature and relative humidity affect SOA formation and key particle properties for an important yet understudied monoterpene, Δ^3-carene.

[a]*Department of Chemistry, Aarhus University, 8000 Aarhus C, Denmark. E-mail: glasius@chem.au.dk; bilde@chem.au.dk*

[b]*Institute for Atmospheric and Earth System Research (INAR), University of Helsinki, 00014 Helsinki, Finland*

[c]*Department of Chemistry and Molecular Biology, University of Gothenburg, 41296 Gothenburg, Sweden*

[d]*Division of Physics, Lund University, 22100 Lund, Sweden*

[e]*Department of Physics, Aarhus University, Aarhus C, 8000, Denmark*

[f]*IVL Swedish Environmental Research Institute, 21119 Malmö, Sweden*

[g]*IVL Swedish Environmental Research Institute, 41133 Gothenburg, Sweden*

† Electronic supplementary information (ESI) available: Placement and sampling cycles of instruments, wall-loss correction, experimental details, background concentration of sulfuric acid, evolution in moderately oxygenated species, details of the offline analysis, time-evolution plots of ozonolysis products (PDF). See DOI: https://doi.org/10.1039/d3ea00128h

‡ These authors contributed to the manuscript equally.

1 Introduction

Secondary organic aerosol (SOA) constitutes a significant fraction of organic particulate matter in the atmosphere[1] and affects climate[2,3] and human health.[4] An important source of SOA is biogenic volatile organic compounds (BVOCs),[1,3,5] *e.g.* monoterpenes including α-pinene and Δ^3-carene. The total annual emission of monoterpenes is estimated to be ~127 Tg C per year, where α-pinene is estimated to account for ~50 Tg C per year.[6] Globally, Δ^3-carene is estimated to have lower emission than α-pinene,[7] but in some environments like the boreal forest, the emission is similar to α-pinene.[8,9] BVOCs are rapidly oxidised in the atmosphere *via* reactions initiated by O_3, NO_3, OH and may be further oxidised by autoxidation.[3,10–12] Oxidation

of BVOC leads to products with volatilities spanning several orders of magnitude,[12,13] often described by the volatility framework and volatility classes developed by Donahue *et al.*[13]

Extremely low volatile organic compounds (ELVOCs) condense onto essentially any existing aerosol particle surface.[12,13] Highly oxygenated organic molecules (HOM), are compounds formed *via* autoxidation, which include at least 6 oxygen atoms.[13] A substantial fraction of HOM formed from monoterpenes, such as the dimers $C_{18-20}H_{28-32}O_{10-18}$, are likely ELVOCs. Since the discovery of HOM in 2014, they have been investigated due to their significant contribution to both formation and further growth of SOA.[10,12,14–16] These compounds are detected with online atmospheric pressure inlet mass spectrometers.[12] In the particle phase, covalently bonded dimers of carboxylic acid monomeric units are identified [*e.g.* ref. 17–26] and their molecular formulae indicate that they also classify as ELVOCs. These dimers have been hypothesised to form in the gas phase perhaps involving $RO_2 + RO_2$ chemistry or stabilised Criegee intermediates,[24,27,28] through esterification[19,29,30] or oligomerisation[18,31] in the particle phase or most recently through acyl peroxy radicals for the C_{15}–C_{19} particle phase dimers.[32] These compounds are identified using offline mass spectrometric methods, such as liquid chromatography coupled to mass spectrometry [*e.g.* ref. 22, 25, 26 and 33–35].

Semi-volatile organic compounds (SVOCs) partition between the gas and the particle phase and therefore exist in considerable fractions in both phases. SVOCs include compounds such as organic acids [*e.g.* ref. 25, 26 and 36–38]. These compounds have been identified with offline mass spectrometric methods since the 1990s[17,36,39] and more recently with online spectrometric methods like the filter inlet for gases and aerosols and chemical ionisation mass spectrometers (FIGAERO-CIMS).[40]

The most-emitted monoterpene α-pinene and its SOA formation has been studied for more than 25 years [*e.g.* ref. 17, 36 and 41–44], but new findings still occur [*e.g.* ref. 25, 26 and 45–49] in particular at low temperatures. Kristensen *et al.*[25,26] observed that the SOA formation from α-pinene is strongly dependent on temperature with decreasing temperatures yielding a higher particle number concentration and a higher particle mass concentration in the temperature range from −15 to 20 °C. Later studies investigated the temperature effects on HOM formation and found that it decreases with decreasing temperature both in the range from −15 to 20 °C[45] and from −50 to 25 °C.[46] Surdu *et al.*[49] investigated the effect of relative humidity on SOA yield and chemical composition from ozonolysis of α-pinene at −10 and −30 °C. They observed an increase in the SOA yield with increasing relative humidity and attributed this enhancement to increased partitioning of semi-volatile organics.

The emission of Δ^3-carene can be almost as large as the emission of α-pinene in boreal forests.[8] In contrast to α-pinene SOA, the SOA formation from Δ^3-carene has only received little attention.[34–36,42,50,51] Previously, the SOA formation from Δ^3-carene has been assumed to be analogous to the SOA formation from α-pinene,[52] because of the similarities in their chemical structures. In a series of experiments in the Aarhus University Research on Aerosol (AURA) atmospheric simulation chamber, Thomsen *et al.*,[34] however, find differences in the formation of SOA from α-pinene and Δ^3-carene. Ozonolysis of Δ^3-carene results in increased particle mass concentrations and larger particles compared to ozonolysis of α-pinene under similar experimental conditions.[34]

The formation of SOA from monoterpenes is affected by environmental conditions like temperature[25,26,45,46] and relative humidity.[42,53,54] The effects of temperature[34,42] and humidity[42,55] on the SOA formation from oxidation of Δ^3-carene were previously studied at different VOC loadings. The SOA yield and the particle number concentration from ozonolysis of Δ^3-carene increased with decreasing temperature at 25 and −30 °C[43] and from 20 to 0 °C.[34] Jonsson *et al.*[42] reported a small increase in the particle mass concentration and particle number concentration with increasing RH, whereas Li *et al.*[55] found that the particle number concentration decreases with increasing RH, while the particle mass concentration is relatively constant. HOM formation from Δ^3-carene oxidation is still understudied[55] and more research is needed to understand the processes and effects of temperature and RH on HOM formation. Furthermore, the volatility distribution of oxidation products from Δ^3-carene has not been studied.

Here, we present an overview of a measurement campaign carried out at the AURA atmospheric simulation chamber to further elucidate the oxidation and aerosol formation from the dark ozonolysis of Δ^3-carene: the Aarhus Chamber Campaign on Evaporation, Partitioning, and Terpene Oxidation, ACCEPTO. We discuss particle phase properties and composition with a focus on the influence of temperature and relative humidity. For the first time, the chemistry and SOA formation during Δ^3-carene ozonolysis is modelled with the Aerosol Dynamics and Gas- and Particle-Phase Chemistry Kinetic Multilayer Model (ADCHAM)[56] and compared to the experimental results from the AURA atmospheric simulation chamber. The formation of HOM and the partitioning of volatile organic products are presented in two separate accompanying papers.

2 Methods

2.1 Chamber experiments

Dark ozonolysis experiments of Δ^3-carene were performed in the AURA atmospheric simulation chamber. Kristensen *et al.*[25] provide a detailed description of the specifications of AURA. In short, AURA consists of a ∼5 m^3 cuboid Teflon bag fixed in a temperature-controlled room. The temperature inside the chamber may be regulated from −16 °C to 26 °C. All instruments used in the current study were placed outside the chamber in an air-conditioned laboratory at 22 °C. The general experimental procedure was (1) filling the chamber with clean air using a zero-air generator (model 737-14, Aadco Instruments, Inc.), (2) injecting ∼180 ppb O_3 using an ozone generator (model 610, Jelight Company, Inc.), and (3) injecting 10 or 20 ppb Δ^3-carene ((+)-3-carene, Sigma-Aldrich, 98.5%) to the AURA chamber through a glass manifold with a heated (>30 °C) flow of nitrogen gas (10 L min^{-1}). Experiment time 0 minutes corresponds to injection of Δ^3-carene marking the start of the

experiment. The initial VOC concentration in ppb is calculated based on the injected volume of Δ^3-carene. Table 1 presents an overview of the Δ^3-carene ozonolysis experiments performed during the ACCEPTO campaign.

The temperature and RH were measured in the centre of the chamber with a probe (HC2-C04, Rotronic AG). Five additional temperature sensors (ADT740, Analog Devices) measured the temperature at five different locations inside the temperature-controlled room around the chamber to check for a uniform temperature throughout the chamber. The ozone concentration and the concentrations of nitrogen oxides (NO and NO_2) were monitored with a UV photometric (O342 Module, Environnement S. A.) and a chemiluminescent monitor (AC32M, Environnement S. A.), respectively.

Particle size distributions were measured with a scanning mobility particle sizer (SMPS) consisting of an electrostatic classifier (model 3082, Impactor 071CM, TSI Inc.) and a water-based condensation particle counter (CPC, model 3788, TSI Inc.). The electrostatic classifier was equipped with a long differential mobility column and operated with a Kr-85 neutraliser (TSI 3077A, TSI Inc.). The SMPS sampling time was 120 s (117 s upscan, 3 s downscan) with a purge time of 30 s to avoid carry-over of particles between scans. The sheath flow was 6.0 L min^{-1} and the aerosol flow was 0.6 L min^{-1}. The lower cut-off diameter was 10 nm and the upper cut-off diameter was 421 nm. In experiments 10D and 10E, the aerosol stream was dried to an RH < 15% with a silica diffusion dryer (TSI Inc.) before entering the SMPS. The initial nucleation was monitored with a nano condensation nucleus counter (nCNC, Model A11, Airmodus Ltd.[57]) consisting of a particle size magnifier (Model A10, Airmodus Ltd.) and a butanol-operated CPC (Model A20, Airmodus Ltd.). The saturator flow was 0.245 L min^{-1} corresponding to a lower cut-off diameter of 1.7 nm. The nCNC measured for 30 minutes and was then disconnected from AURA. The chemical composition of the particles was monitored in several ways: (1) with a high-resolution time-of-flight aerosol mass spectrometer (AMS, Aerodyne Research, Inc.[58]), (2) with a Filter-Inlet for Gases and AEROsols Chemical Ionization Mass Spectrometer (FIGAERO-CIMS[40]), and (3) using a sequential spot sampler (Series 110 A, Aerosol Devices[59,60]) for detailed offline analysis using an ultra-high performance liquid chromatograph coupled to a mass spectrometer through an electrospray ionization inlet. The AMS was operated in V-mode with 1 minute averaging and a flow rate of 0.08 L min^{-1}. In experiments 10D and 10E, the aerosol stream was dried before entering the AMS with an aerosol dryer (Aerodyne Research, Inc.). The gas phase was monitored with (1) a chemical ionization atmospheric pressure interface time-of-flight mass spectrometer (NO_3-CIMS)[61,62] and (2) the FIGAERO-CIMS. An overview of the instrument positions around the AURA chamber, the flows, and their sampling cycles are given in Section 1 in the ESI.† Experiment 10C was performed after the campaign without the FIGAERO-CIMS and the NO_3-CIMS. To maintain similar flow conditions in the chamber without these instruments sampling as in the previous experiments, a pump with a similar flow to these two instruments removed air from the chamber to simulate sampling from the instruments.

All particle number concentrations are reported without wall-loss correction. All particle mass concentrations measured with the SMPS are wall-loss corrected according to Pathak *et al.*[63] with an optimised fit of the decay of particle mass concentration. Section 2 in the ESI† describes the optimised fit and the following wall-loss correction. The uncertainty on the ozone concentration was estimated from the noise and the accuracy associated with the instrument. The uncertainty on the initial concentration of the VOC was estimated from previous experiments[34,35] where the VOC concentration was measured with a proton transfer reaction mass spectrometer or a gas chromatograph with a flame ionisation detector. The absolute uncertainty for these experiments was 5 ppb, which is then also expected to be the same during the ACCEPTO campaign and it brings a noticeable uncertainty to the estimated SOA yields. The SOA yields are calculated according to Odum *et al.*[64] and Pathak *et al.*[63] The SOA yields are based on the aimed initial VOC

Table 1 Experimental conditions for the ozonolysis experiments performed in the ACCEPTO campaign. The maximum particle mass concentrations are reported after wall-loss correction. The VOC starting concentration, $[VOC]_0$, is calculated based on the injected volume of Δ^3-carene. The absolute uncertainty on the Δ^3-carene concentration is based on previous measurements.[34,35] The uncertainty in the O_3 concentration is estimated based on the noise and instrument accuracy. The uncertainty on the SOA yield is based on the uncertainty of the SMPS measurements and the absolute uncertainty of the Δ^3-carene concentration

						Max. concentrations		
Date	ID	$[VOC]_0$ (ppb)	$[O_3]_0$ (ppb)	T_{avg} (°C)	RH_{avg} (%)	Number ($\times 10^4$ cm^{-3})	Mass (μg m^{-3})	SOA yield (%)
220202	0A	10 ± 5	159 ± 15	0.1 ± 0.1	1.6 ± 1.6	3.1	3.1	5 ± 3
220113	10A	10 ± 5	174 ± 15	10.1 ± 0.1	0 ± 0	2.9	3.2	7 ± 4
220204	10B	10 ± 5	171 ± 15	10.1 ± 0.1	0.4 ± 0.8	3.8	7.4	13 ± 7
220427	10C[a]	10 ± 5	169 ± 15	10.2 ± 0.1	0.6 ± 1.0	2.7	5.7	9 ± 5
220124	10D	10 ± 5	174 ± 15	10.2 ± 0.1	78 ± 2	18.1	3.6	4 ± 2
220131	10E	20 ± 5	169 ± 15	10.2 ± 0.1	76 ± 1	17.2	20.6	14 ± 7
220111	20A	10 ± 5	181 ± 15	20.2 ± 0.1	0 ± 0	2.9	5.5	9 ± 5
220205	20B	10 ± 5	181 ± 15	20.2 ± 0.1	0 ± 0	3.3	7.4	11 ± 6

[a] This experiment was performed after the main campaign and a pump was added to simulate the airflows of the FIGAERO-CIMS and the NO_3-CIMS.

concentrations of 10 ppb and the assumption that all Δ^3-carene is consumed.[34] The nucleation rate is calculated as described in Tomicic *et al.*[65] and the growth rate for particles with diameter > 20 nm is calculated according to Kulmala *et al.*[66] using the maximum-concentration method.[67] An outlier test was performed for the mass fraction at 90 min acquired in the offline analysis in experiment 20A. The outlier test followed Fisher's least significance difference method described in Su *et al.*[68]

2.2 Particle sampling and offline analysis

Particle samples were collected continuously with a sequential spot sampler (Series 110 A, Aerosol Devices)[59,60] in 30 minute intervals at a flow rate of 1.25 L min^{-1}. The sequential spot sampler was operated with the following settings: conditioner temperature of 5 °C, initiator temperature of 35 °C, moderator temperature of 8 °C, nozzle temperature of 27 °C, and sample plate temperature of 35 °C. The particle samples were first extracted with 10% acetonitrile in MilliQ water (<0.05 μS cm^{-1}), then with 50% acetonitrile in MilliQ water. The particle extracts were stored at 5 °C until analysis. The analysis was performed according to Thomsen *et al.*[35] with an ultra-high performance liquid chromatograph (UHPLC) coupled to a quadrupole time-of-flight mass spectrometer (QTOF-MS, Compact, Bruker) through an electrospray inlet. The UHPLC method and QTOF-MS settings are described briefly in Section 6 in the ESI† and a detailed description is found elsewhere.[34] Ozonolysis products of Δ^3-carene are tentatively identified with authentic standards of α-pinene oxidation products by analyzing their compound-specific retention times[34,36] and their mass spectral information *e.g.* fragmentation patterns and the molecular ions, $[M-H]^-$.[19,21,23,24,69,70] The α-pinene oxidation product standards were: *cis*-pinic acid (Aldrich), *cis*-pinonic acid (Aldrich, 98%), and diaterpenylic acid acetate (DTAA, kindly supplied by Y. Iinuma, TROPOS, Leipzig, Germany). Due to an extraction error, the data from particle samples from experiment 20B are not reported.

2.3 FIGAERO-CIMS

A High-Resolution Time-of-Flight Chemical Ionisation Mass Spectrometer (HR-ToF-CIMS) combined with a Filter Inlet for Gases and AEROsols (FIGAERO, Aerodyne Research Inc.) was connected to the AURA chamber to measure both gas and particle phase oxidation products. A more detailed description of HR-ToF-CIMS with a FIGAERO inlet is found in Lopez-Hilfiker *et al.*[40] During the ACCEPTO campaign, the flow rate of the gas phase into the ion molecule region (IMR) was 2 L min^{-1}. Simultaneously, the particle phase sample was collected on PALL® PTFE membrane filter for 10 min with a flow of 3 L min^{-1}. Fig. S.2† shows the sampling cycle of the FIGAERO-CIMS. The particle sample was subsequently desorbed by heated pure N_2 (2 L min^{-1}) into the IMR. The iodide (I^-) ion produced from the ionisation of methyl iodide (CH_3I) was delivered into the IMR in a flow of pure N_2. The reagent ion (I^-) and targeted compounds form molecular adduct ions in IMR and the adducts were detected by the HR-ToF-CIMS. The partitioning of detected compounds was calculated using the ion counts in the gas phase and the corresponding ion counts in the particle phase.

2.4 Nitrate-CIMS

A NO_3-CIMS (Tofwerk AG/Aerodyne Research, Inc.[62]) with nitrate (NO_3^-) as reagent ions were deployed for measuring highly oxygenated products of Δ^3-carene oxidation in the gas phase. The sample molecules are detected either as deprotonated ions ($[M-H]^-$) or more typically as clusters with reagent ions ($M\cdot NO_3^-$). The instrument was configured to be capable of determining ions up to 960 Th with a mass resolving power of ~8500 Th. In all experiments, except 10A and 20A, the instrument sampled 10 L min^{-1} from the chamber for the first 80 min after Δ^3-carene injection, after which a cycle was started with 40 min without sampling alternating with 20 min of sampling. This was done to limit the amount of air drawn from the chamber. Fig. S.2† shows the sampling cycle of the CI-APi-TOF. In experiments 10A and 20A, air from the chamber was sampled with a flow rate of 5 L min^{-1} and directly mixed with an equally large clean airflow. In these cases, the sampling was continuous throughout the experiments. The NO_3-CIMS data were pre-processed with tofTools MATLAB package (version 612).[71]

2.5 ADCHAM modelling

The Aerosol Dynamics and Gas- and Particle-Phase Chemistry Kinetic Multilayer Model ADCHAM[72] was used to simulate the gas phase chemistry and secondary aerosol formation during selected ACCEPTO experiments. ADCHAM considers wall losses of particles and gases to the chamber walls and all aerosol dynamic processes. The particle number size distribution was represented by 200 size bins between 1.7 nm and 516 nm in diameter. Currently, no complete gas phase chemistry mechanism for ozonolysis and OH oxidation of Δ^3-carene exists. Thus, in this work, we developed and implemented a Δ^3-carene oxidation mechanism which is based on the Master Chemical Mechanism v3.3.1 (MCMv3.3.1) for α-pinene chemistry[73,74] and the Peroxy Radical Autoxidation Mechanism (PRAM).[75,76] The first reaction steps of the O_3 and OH oxidation of Δ^3-carene is represented by the mechanisms proposed by Wang *et al.*[79] and Hantschke *et al.*,[77] using the temperature-dependent Δ^3-carene + OH reaction rate constant from Dillon *et al.*:[78] 2.48×10^{-11} $\exp(357/T)$ cm^3 $molecule^{-1}$ s^{-1}. We could not find any empirically derived temperature-dependent reaction rate constant for ozonolysis of Δ^3-carene in the literature. Hence, in this work we assume that the temperature-dependence for the Δ^3-carene + O_3 reaction rate constant is the same as for α-pinene in MCM: $3.7 \times 10^{-16} \exp(-640/T)$ cm^3 $molecule^{-1}$ s^{-1}. The implemented Δ^3-carene + O_3 reaction rate constant matches the reaction rate constant reported by Hantschke *et al.*[77] at 300 K. The OH yield from the ozonolysis of Δ^3-carene in the mechanism is 65%, which was based on the empirically estimated yield from Hantschke *et al.*[77] of 65%. It can also be compared with the theoretical values of 56–59% from Wang *et al.*[79] To be able to represent the observed HOM mass spectrum in ADCHAM we used a total ozonolysis molar yield of 2.5% for the first RO_2 isomers ($C_{10}H_{15}O_4$) that can undergo autoxidation and produce

HOM in PRAM. In addition, we also included a minor (<0.4% molar yield) C_9RO_2 ($C_9H_{13}O_4$) autoxidation pathway to HOM, in order to capture the observed mass peaks corresponding to the ions $C_9H_{12}O_9$ and $C_9H_{14}O_9$. A more detailed description of the new Δ^3-carene gas phase chemistry mechanism is provided in Luo *et al.* (in prep.).

3 Results and discussion

3.1 Particle formation and growth

Fig. 1 shows the formation and growth of particles over time obtained from the SMPS data. The upper panels (I–III) relate to investigating the temperature dependence of the SOA formation from ozonolysis of Δ^3-carene. The lower panels (IV–VI) relate to the investigation of the effect of relative humidity on SOA formation from ozonolysis of Δ^3-carene. Consistent with previous observations,[34,35] the particle number concentration generally increases steeply a few minutes after the injection of Δ^3-carene. After the maximum particle number concentration is reached, a decay ascribed to wall loss and coagulation is observed. The particle mass concentration and particle mode diameter also grow and reach relatively constant values after about 150 minutes. The full experimental details are presented in Section 3 in ESI.†

The particle number concentrations at 0, 10, and 20 °C at 0% RH are in the range (2.7–3.8) $\times$ 10^4 # cm^{-3}. Across all temperatures, the measured particle number concentrations are almost equal. However, the particle mass concentrations in experiments 10A–C and 20A–B fluctuate. This variation in particle mass concentrations – especially pronounced at 10 °C – makes it difficult to draw any firm conclusions in relation to temperature trends, however, this points towards that the temperature effect on ozonolysis of Δ^3-carene is not very strong at the current experimental conditions. The variation in particle mass concentration may in part arise from small differences in the initial concentration of VOC as suggested by the result of the ADCHAM model (Section 3.3) or in part, the low VOC loadings where the concentration of trace compounds, *e.g.* ammonia or sulfuric acid,[80,81] might play a significant role in the formation of particles.

The average particle mode diameter for SOA for all experiments at the maximum particle mass is 80 $\pm$ 9 nm, which again indicates that the temperature does not strongly affect the SOA formation from ozonolysis of Δ^3-carene. Table 2 shows the nucleation rates and growth rates for all experiments. Neither the nucleation rates nor growth rates show a strong temperature dependence under dry conditions and are across all temperatures between 33.8–59.4 # cm^{-3} s^{-1} and 35.1–51.7 nm h^{-1}. In contrast, Simon *et al.*[46] observed increasing nucleation rates with decreasing temperatures for α-pinene oxidation. This illustrates that ozonolysis of Δ^3-carene exhibits a less pronounced temperature dependence compared to ozonolysis of α-pinene under dry conditions.

It is interesting to compare our data with previous observations of ozonolysis of monoterpenes in the AURA simulation chamber.[25,26,34] Ozonolysis of α-pinene exhibits a clear temperature dependence showing increasing particle number concentrations and particle mass concentrations with decreasing temperature at both 10 and 50 ppb.[25,26] However, the temperature effect is less pronounced for the ozonolysis of 10 ppb of α-pinene than at 50 ppb. Ozonolysis of 50 ppb Δ^3-carene show some temperature dependency, but not to the same degree as for ozonolysis of α-pinene.[34] It thus seems reasonable that the lower VOC concentration in this study leads to a weaker temperature effect for ozonolysis of Δ^3-carene. However, drawing any definitive conclusions about the effect of temperature on the particle number concentrations and particle mass concentrations is hindered by the uncertainty in the initial VOC concentration and that only one experiment was performed at 0 °C.

Regarding the influence of relative humidity, ozonolysis of 10 ppb Δ^3-carene at 0% RH (low RH, experiments 10A–C) and at 80% RH (high RH, experiment 10D) result in comparable particle mass concentrations. Meanwhile, the particle number concentrations from ozonolysis of Δ^3-carene at low RH are in the range (2.7–3.8) $\times$ 10^4 # cm^{-3}, while the resulting particle number concentration at the high RH is 18.1 $\times$ 10^4 # cm^{-3}. The drastic increase in the particle number concentration at high RH is also observed in experiment 10E, where ozonolysis of 20 ppb Δ^3-carene at 80% RH results in a similar particle number concentration of 17.2 $\times$ 10^4 # cm^{-3} and a higher particle mass concentration consistent with the increased VOC loading. The high particle number concentrations observed in both experiments at high RH indicate that RH influences nucleation. This is also clear from the nucleation rates (Table 2) for experiments 10D and 10E, which are considerably higher than in the dry experiments.

While we cannot separate individual contributions to nucleation, growth, and resulting particle mass concentration based on these measurements, it is known that humid conditions enhance the nucleation driven by inorganics.[80,82] No inorganics are added to the AURA chamber during these experiments, but direct background measurements show that sulfuric acid is present in very low concentrations (Fig. S.8†). The level of H_2SO_4 is similar in all experiments. However, in experiments with increased RH, water should stabilise the H_2SO_4 clusters leading to higher cluster formation rates compared to dry experiments.[56,83,84]

The particle growth rate is 43 $\pm$ 6 nm h^{-1} at the low RH and 20.6 nm h^{-1} at the high RH. The smaller particle diameter (48 nm) at high RH compared to low RH (80 $\pm$ 9 nm) naturally follows from similar particle mass concentrations but a much higher particle number concentration at high RH.

Previous observations of the effect of RH on SOA formation show conflicting results. Jonsson *et al.*[42] report an increasing particle number concentration with increasing RH in agreement with this work and suggest that it is a mechanistic effect. In contrast, Bonn *et al.*[53] find a decreasing particle number concentration with increasing RH, but do not pursue an explanation of the observation. The discrepancy in the observations may be due to different experimental conditions, as Jonsson *et al.*[42] use ~29 ppb Δ^3-carene and ~2000 ppb O_3 in a flow tube setup, while Bonn *et al.*[53] use 500 ppb of both α-pinene and O_3 in a spherical glass reactor.[85,86]

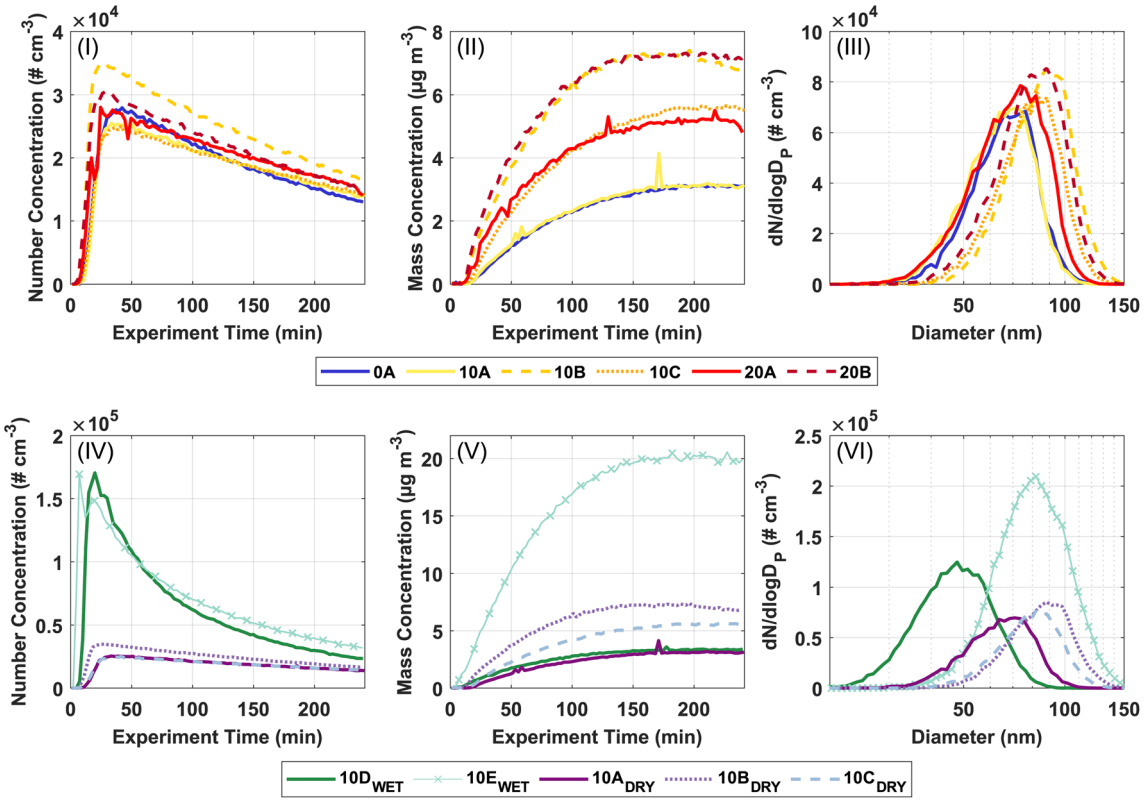

Fig. 1 Panels (I–III) refer to experiments conducted in order to investigate temperature dependence. Panels (IV–VI) refer to experiments conducted in order to investigate the effect of humidity. Experiment $10E_{WET}$ is marked with × as it was performed with a starting concentration of Δ^3-carene of 20 ppb instead of 10 ppb. (I and IV) Particle number concentrations in # cm^{-3}. (II and V) SMPS derived particle mass concentrations in µg m^{-3}. (III and VI) Particle size distributions at maximum particle mass concentration. Note that experiment 10A–C is plotted in both series.

Table 2 Nucleation rates, J_{D_p}, for particles with D_p > 1.7 nm based on the nCNC particle number concentration and growth rates, GR_{D_p}, for particles with D_p > 20 nm based on the SMPS particle number concentration

ID	$J_{1.7}$ (# cm^{-3} s^{-1})	GR_{20} (nm h^{-1})
0A	35.6	35.1
10A	33.8	36.1
10B	59.4	46.1
10C	32.0	46.8
10D	697.2[a]	20.6
10E	1108.3[a]	44.3
20A	40.2	43.9
20B	36.2	51.7

[a] Nucleation rate calculated between the 20% limit and the upper limit of the nCNC.

The effect of humidity is often observed as a considerable increase in the particle mass concentration due to water uptake. During the ACCEPTO experiments carried out at high RH, the particles were dried prior to measurement with the SMPS and the AMS and hence this water uptake is not visible in our observations. Jonsson *et al.*[42] measure the particle size distributions with no drying of the particles and observe an increase in the particle mass concentration. They explain ~30% of their growth with water uptake and state that the additional growth observed is due to a mechanistic effect of water affecting the product distribution.

3.2 Aerosol composition

Three approaches to characterise the aerosol phase have been applied in this study: (1) AMS, (2) FIGAERO-CIMS, and (3) off-line analysis using UHPLC-QTOF-MS. AMS yields information on the general oxidation state of the particle phase in the form of hydrogen-to-carbon (H/C) ratios and oxygen-to-carbon (O/C) ratios. The FIGAERO-CIMS provides information on partitioning. The analysis of particles collected yields both qualitative and quantitative information on aerosol composition.

The O/C ratio is often used to characterize the degree of oxidation of compounds in the particle phase. Fig. 2 shows a van Krevelen plot with the H/C ratio as a function of the O/C ratio from AMS data from each experiment. A slight temperature trend is observed with an increasing O/C ratio with increasing temperature for dry experiments. Previous studies with ozonolysis of Δ^3-carene at 50 ppb[34] and 100 ppb[35] and ozone concentration of about 200 ppb, respectively, both show O/C ratios of about 0.4. In this work, the O/C ratio for experiments 10A–C lies at about 0.45–0.5, which indicates a more oxidised particle phase. This likely stems from the lower VOC loading in this work, while the ozone concentration is similar to the previous studies.[34,35] It seems that there is an effect of relative humidity on the H/C ratio for the ozonolysis of 10 ppb

Δ^3-carene. For the low RH experiments at 10 °C, the H/C ratio is between 1.55 and 1.6; for experiment 10D with high RH, the H/C ratio range between 1.6 and 1.7 over the duration of the experiment. An increasing H/C in ambient AMS measurements has previously been suggested to arise from hydrolysis.[87] However, an increase in the H/C ratio for ozonolysis of 20 ppb Δ^3-carene at 80% RH (10E) is not observed, which might suggest that the increase in H/C ratio for the ozonolysis of 10 ppb Δ^3-carene does not arise from hydrolysis. The O/C ratio is either similar (10D) or lower (10E) at high relative humidity compared to dry conditions (10A-C). Surdu *et al.*[49] observe decreasing O/C ratios with increasing RH. This decrease in O/C is suggested to arise from an increase in moderately oxygenated compounds ($C_{10}H_{16}O_{2-5}$), while more oxygenated compounds ($C_{10}H_{16}O_{6-8}$) are unaffected. No such effect is observed in offline chemical analysis (Fig. 4) nor in the online measurements from the FIGAERO (Fig. S.9†).

In the offline analysis, four carboxylic acids, *cis*-3-caric acid, *cis*-3-caronic acid, OH–3-caronic acid (10-hydroxy-3-caronic acid), and a carboxylic acid with molecular weight (MW) 170 g mol^{-1}, are tentatively identified. MW170 is tentatively identified as 3-caralic acid or nor-3-caronic acid.[34] In addition to the four carboxylic acids, one dimer with MW 368 g mol^{-1} was tentatively identified. The presence of these five ozonolysis products is in line with previous work,[34] where Thomsen *et al.* identified ~50% of the total particle mass and find that ~2/3 of the identified particle mass arise from *cis*-3-caric acid in SOA formed from ozonolysis of 50 ppb Δ^3-carene. Fig. S.10† shows the development of the estimated concentrations of ozonolysis products *cis*-3-caric acid and *cis*-3-caronic acid over time in experiments 0A, 10A, 10B, 10C, and 20A as mass fractions compared to the SMPS particle mass concentration without wall-loss correction. Mass fractions are presented in order to avoid overinterpretation of mass differences between experiments and to indirectly correct for wall loss. A substantial mass fraction of *cis*-3-caric acid (~30%) is found in the particle phase.

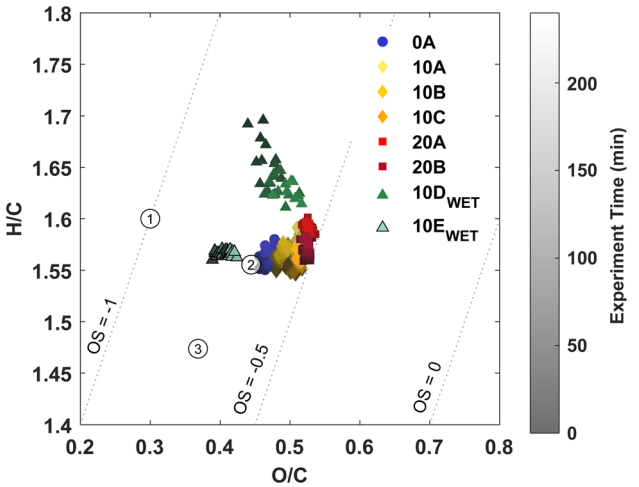

Fig. 2 A van Krevelen plot with the general oxidation state of the particle phase. Three oxidation states of known compounds from ozonolysis of Δ^3-carene are shown. (1) *cis*-3-Caric acid, (2) *cis*-3-caronic acid, and (3) dimer MW368.

The condensation of *cis*-3-caric acid has previously been suggested to be more efficient than *cis*-pinic acid,[34] which might explain this large fraction of *cis*-3-caric acid in the particle phase. Fig. S.12† shows the development in the mass fractions of OH–3-caronic acid and the estimated mass fraction of MW170. OH–3-caronic acid constitutes ~10% of the particle mass. MW170 is only detected in experiments 10B and 10C after 90 minutes. A gradual build-up from 0.1% of the total particle mass to 1.4% of the total particle mass is observed.

Fig. 3 shows the mass fractions of the ozonolysis products *cis*-3-caric acid, *cis*-3-caronic acid, and OH–caronic acid for experiments 0A, 10A, 10B, 10C, and 20A. The correlation coefficients, R^2, from linear least squares regression were between 0.68 and 0.92 at 0 and 20 °C. Overall, an increase with time in the mass fraction of *cis*-3-caric acid, *cis*-3-caronic acid, and OH–3-caronic acid is observed at 0 °C. In contrast, at 20 °C, a decrease of *cis*-3-caric acid, *cis*-3-caronic acid, and OH–3-caronic acid is observed. At 10 °C, no apparent trend is observed. This is consistent with R^2 generally being lower for 10 °C experiments. It is interesting that the fractions of the three carboxylic acids increase with time at 0 °C, while the fractions decrease with time at 20 °C. This suggests that condensation of the three carboxylic acids is continuous at lower temperatures, while at higher temperatures, evaporation back into the gas phase or further reactions removing these species are favourable, and other reaction products not detected by the present analysis become more prominent in the particle phase.

Fig. 4 shows the development in the mass fractions of *cis*-3-caric acid and *cis*-3-caronic acid over time in experiments 10A–E to investigate the effect of RH. Ozonolysis of 10 ppb Δ^3-carene at 0% RH results in a mass fraction of *cis*-3-caric acid between 10 and 35%, while ozonolysis of 10 ppb Δ^3-carene at 80% RH results in a mass fraction of *cis*-3-caric acid between 10 and 70%. After 90 minutes, the mass fraction of *cis*-3-caric acid formed at 80% RH exceeds the mass fraction of *cis*-3-caric acid formed at 0% RH. The increase in *cis*-3-caric acid could potentially be linked to enhanced partitioning of *cis*-3-caric acid as the bulk diffusivity increases and the viscosity decreases with increasing RH.[49]

Surprisingly, we observe that the mass fraction of *cis*-3-caronic acid found in the particle phase at 80% RH is lower than the mass fraction of *cis*-3-caronic acid at 0% RH. Surdu *et al.*[49] discussed the effect of water on the gas-particle partitioning of semi-volatiles in detail. Water vapour tends to have little effect on the gas phase chemistry, but if water were to react with a Criegee intermediate a higher concentration of *cis*-3-caronic acid would be expected. They deem this a negligible contribution in good agreement with our observations of a lower mass fraction of *cis*-3-caronic acid with increasing RH. Ma *et al.*[88] found that the formation of *cis*-pinonic acid from ozonolysis of α-pinene is indeed water dependent and Tillmann *et al.*[54] stress that the effect of water on the oxidation products from α-pinene is not understood to fully describe the effects on the SOA formation and its dependency on water. Tillmann *et al.*[54] also observe a humidity-dependent gain in SOA yields at −20 and −30 °C and explain the growth as arising from water-dependent chemistry in the formation of oxidation products and rule out physical water uptake. Fig. S.12† shows the development over

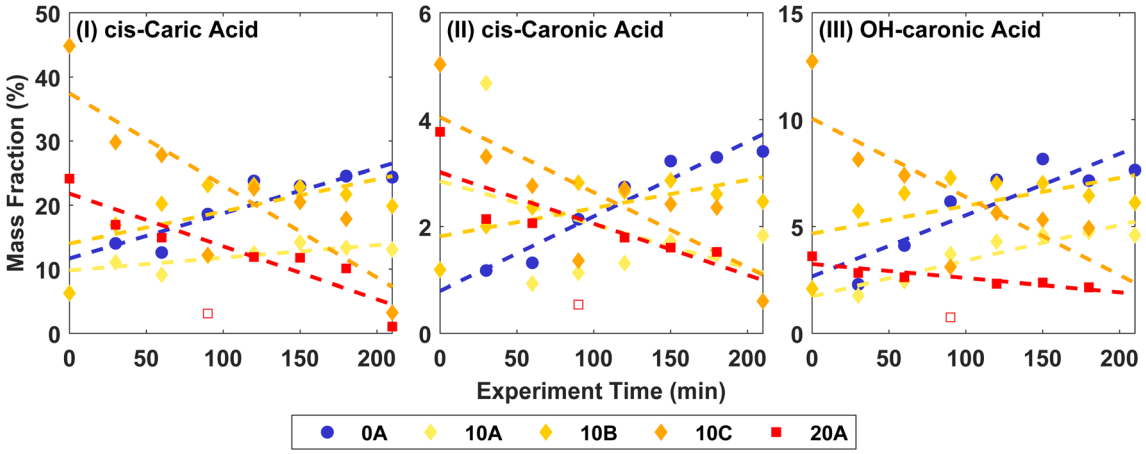

Fig. 3 Mass fractions of (I) *cis*-3-caric acid, (II) *cis*-3-caronic acid, and (III) OH–3-caronic acid at 0, 10, and 20 °C. The dashed lines show linear least squares regression to the experimental data, where the open point for 20A is omitted in the fit as it is an outlier (Fisher's least significance difference method,[68]).

time of OH–3-caronic acid for experiments 10A–E. No effect of humidity is observed for the presence of OH–3-caronic acid in the particle phase. Meanwhile, MW170 is only observed in the low RH experiments 10B and 10C and also in the high RH experiment with the higher VOC loading, 10E. These somewhat contradictory observations for four semi-volatile oxidation products stress that it is important to study the effect of humidity on oxidation pathways of BVOCs and the subsequent SOA formation and growth.

3.3 Modelling

According to the ADCHAM simulations, approximately 1/3 of all Δ^3-carene was oxidised by OH and 2/3 by O_3 in the dry experiments 20A–B, 10A–B and 0A. At the start of the experiments, the

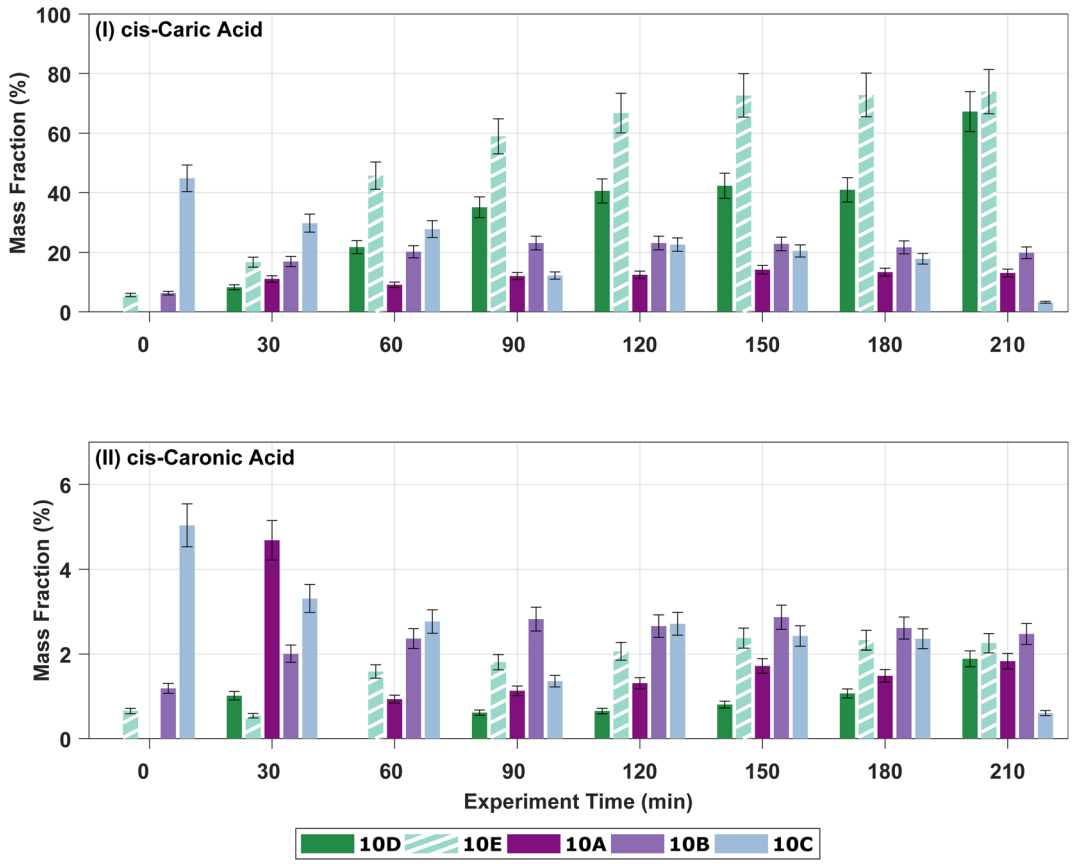

Fig. 4 Mass fractions of ozonolysis products of Δ^3-carene at 0% RH (10A–C) and 80% RH (10D–E). (I) The evolution over time of *cis*-3-caric acid with an estimated uncertainty of ±10%. (II) The evolution over time of *cis*-3-caronic acid with an estimated uncertainty of ±10%.

modelled maximum OH concentration was in the range (1.0–1.4) $\times$ 10^6 molecules cm^{-3}. The highest OH concentrations were reached in the 20A–B experiments and the lowest in the 0A experiment. In all simulated experiments, more than 90% of all Δ^3-carene was consumed within 3 hours.

Fig. 5(I) and (II) show both the modelled and measured ozone concentrations for experiments 10A and 10B. From the measured ozone concentration, an initial Δ^3-carene concentration is estimated as the ozone decay at the beginning of an experiment depends on the Δ^3-carene concentration. The estimated initial Δ^3-carene concentrations for experiments 10A and 10B are 6.5 and 14 ppb, respectively. The estimated absolute uncertainty of the Δ^3-carene concentration of 5 ppb gives a range of Δ^3-carene concentrations spanning from 5 to 15 ppb. For this range of initial Δ^3-carene concentrations, the model predicts ozone concentrations as outlined by the shaded area in Fig. 5. The calculated initial Δ^3-carene concentrations are both within the estimated uncertainty on the injected amount of Δ^3-carene. By using the estimated initial Δ^3-carene concentrations, the model is able to reproduce the measured ozone concentration apart from spikes and scattering of the data. In both experiments, the ozone concentration decreases faster after about two hours. This is expected to arise from leaks of surrounding air into the chamber and therefore included in the ADCHAM model as a dilution factor. Fig. 5(III) shows the modelled SOA mass concentration and the AMS mass concentration. The modelled results are based on the estimated initial Δ^3-carene concentrations of 6.5 and 14 ppb for experiments 10A and 10B, respectively. The shaded area represents model predictions of the full range of possible initial Δ^3-carene concentrations according to the absolute uncertainty related to the concentration. With the estimated Δ^3-carene concentration, the ADCHAM model captures the evolution in the SOA mass concentration within the experimental uncertainties. The model results from experiments 0A, 20A and 20B are presented in Section 7 in the ESI.† At both 0 and 20 °C, both the ozone concentrations and the SOA mass concentrations are captured by the model in agreement with experiments 10A and 10B.

The modelled SOA mass yields are generally higher than the experimentally derived values shown in Table S.1.† This is expected because the modelled SOA yields use the actual consumed amount of Δ^3-carene estimated by the model, while the experimentally derived SOA yields assume that the consumed concentration of Δ^3-carene is 10 ppb.

The modelled, particle wall-loss corrected SOA yields range from 11 (20A) to 20% (10B) and are influenced both by the temperature and the amount of reacted Δ^3-carene. SOA yields generally decrease with increasing temperature and increase with the amount of reacted VOC [*e.g.* ref. 25, 26, 34, 43, 63 and 89]. According to the modelled ozone trends, it is likely that experiments 0A and 10A had lower initial Δ^3-carene concentrations, $\sim$5 and $\sim$6.5 ppb, respectively, while experiments 10B and 20B had higher initial Δ^3-carene concentrations, $\sim$14 ppb (Fig. 5, S.14 and S.15†). We also used the model to calculate SOA mass yields for an idealised atmospheric simulation chamber without dilution and wall losses of particles and gases. These modelled, atmospherically relevant SOA mass yields range between 16% at 20 °C and 32% at 0 °C for experiments where 10 ppb Δ^3-carene is oxidised by ozone and OH without the presence of UV light.

Consistent with the observations, the modelled relative SOA mass fractions of *cis*-3-caric acid and OH–3-caronic acid increased with decreasing temperatures. The *cis*-3-caric acid mass fractions ranged between 17% and 26% and the OH–3-caronic acid mass fractions between 2% and 5% at the end of the experiments. Meanwhile, *cis*-3-caronic acid has a negligible contribution to the modelled SOA mass, except for experiment 0A where *cis*-3-caronic acid contributes to 2% of the SOA mass. The modelled SOA O/C ratios were 0.58–0.60 in experiments 20A–B, 0.52–0.55 in experiments 10A–B and 0.50 in experiment 0A. Thus, it is mainly in the 20A–B experiments that the model O/C ratios are substantially higher than the observed experimental values (Fig. 2).

3.4 Highly oxygenated organic molecules

HOMs are produced rapidly *via* autoxidation after injecting Δ^3-carene into the AURA chamber. Most HOMs are low or extremely low-volatility organic compounds (ELVOCs), and they can both form new particles and condense onto chamber walls or particles contributing to further particle growth.[10,12,90] Therefore, the observed HOM concentrations in the chamber are the results of the balance between formation and loss. A variety of products in the gas phase were detected by the NO_3-CIMS, including both HOM monomers mostly with 8–10 carbon atoms and HOM dimers with 18–20 carbon atoms.

Fig. 6 shows the time series of two selected HOM monomers $C_{10}H_{14}O_9$ and $C_{10}H_{16}O_9$ in experiments 20B, 10B, and 0A. At the beginning of each experiment, HOM are rapidly produced while the condensation sink from new particles is still low, thus we find $C_{10}H_{14}O_9$ and $C_{10}H_{16}O_9$ grow by more than an order of magnitude within 10 min. After around 20 min, $C_{10}H_{14}O_9$ and $C_{10}H_{16}O_9$ start to decrease because of the increasing condensation sink and loss rate of HOM.

The autoxidation of RO_2 to form HOM is temperature dependent, where low temperatures decrease the autoxidation process, and hence are expected to result in less HOM formation.[91,92] From Fig. 6, it is clear that the temperature at which the Δ^3-carene ozonolysis took place had a considerable impact on the HOM concentrations. The signal intensities of $C_{10}H_{14}O_9$ and $C_{10}H_{16}O_9$ were up to one order of magnitude higher at 20 °C compared to 0 °C 10 min after the injection of Δ^3-carene. A similar result with an even stronger enhancement of HOM formation at 20 °C was found for ozonolysis of α-pinene by Quéléver *et al.*[45] The relative abundance of $C_{10}H_{14}O_9$ and $C_{10}H_{16}O_9$ signals increase slightly with decreasing temperatures indicating the potentially different distributions of HOM at different temperatures. More details of HOM formation and the influence of temperature and RH will be reported in a following paper.

3.5 Partitioning of 3-caronic acid

From the high-resolution peak fitting of the collected FIGAERO-CIMS dataset, one of the dominant detected compounds is

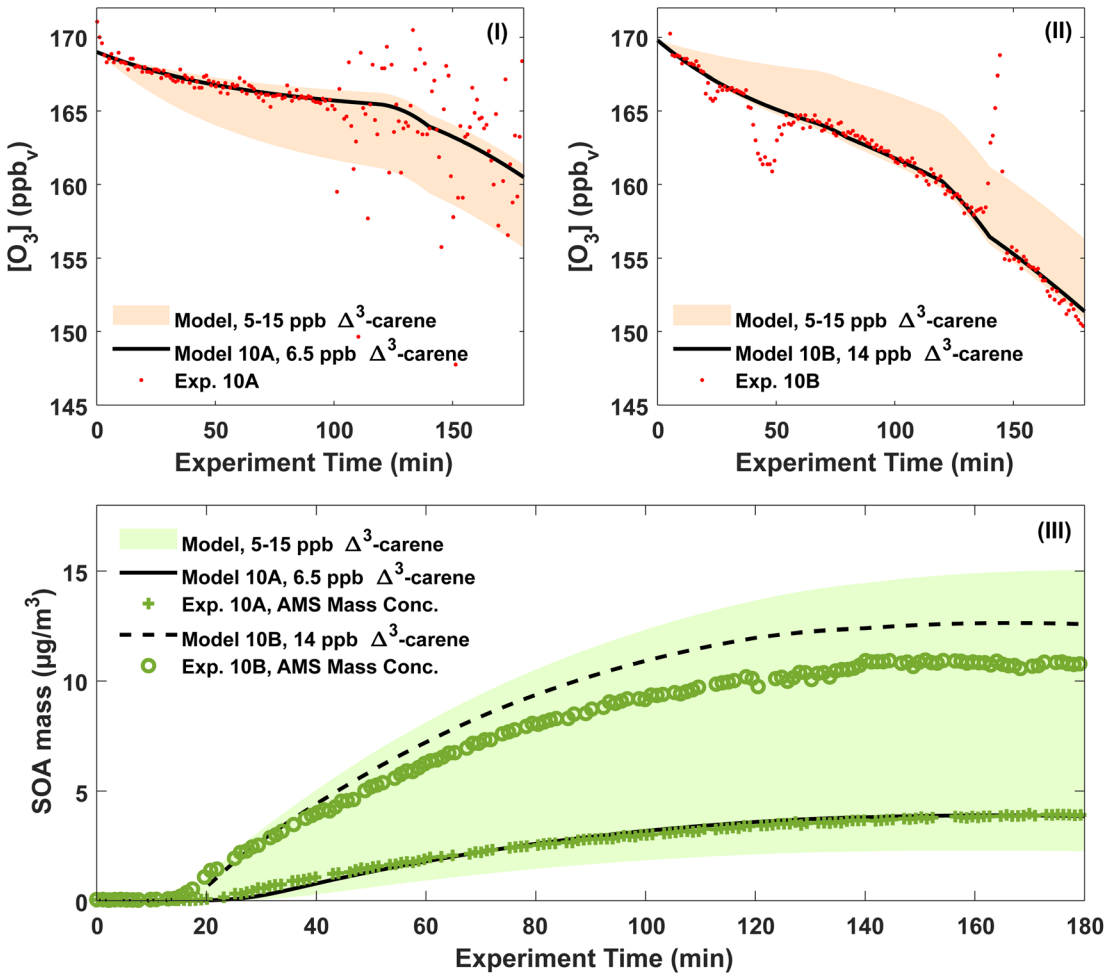

Fig. 5 (I and II) Measured and modelled ozone concentrations in experiments 10A and 10B. The ozone concentrations were used to calculate initial Δ^3-carene concentrations of 6.5 ppb and 14 ppb for experiments 10A and 10B respectively. (III) The measured and modelled SOA mass concentrations for experiments 10A and 10B. The model assumes initial concentrations as calculated from the ozone concentrations.

$C_{10}H_{16}O_3$. The time trends of $C_{10}H_{16}O_3$ in the gas and particle phases of experiments 0A and 20B are shown in Fig. 7. The molecular formula ($C_{10}H_{16}O_3$) may have different structures, *e.g.* isomers which FIGAERO-CIMS cannot distinguish, but this molecular formula corresponds to caronic acid, one of the dominant products from Δ^3-carene ozonolysis as also identified

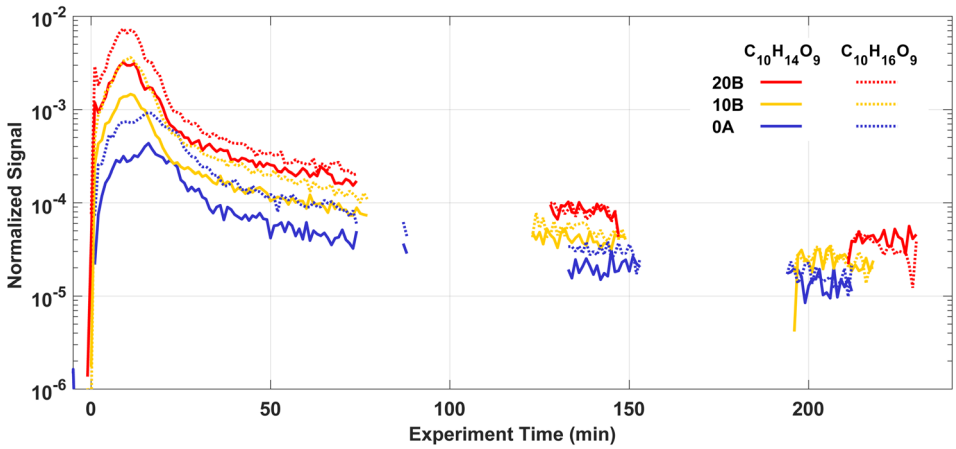

Fig. 6 Temporal behaviours of two main HOM monomers: $C_{10}H_{14}O_9$ and $C_{10}H_{16}O_9$ from Δ^3-carene ozonolysis at different temperatures. Signal intensities were normalised to the signal of reagent ions. Data were averaged over 1 min. Periods without signal correspond to the sampling cycle of the NO_3-CIMS.

in the offline analysis (Fig. 4 and S.10†). Thus, here $C_{10}H_{16}O_3$ is discussed as *caronic acid*. The total signals of caronic acid increase with experiment time and peak at around 2 h and then decrease, primarily due to wall loss of both particles and gases in the chamber. Comparison of experiments 0A and 20B shows that an increase in temperature leads to an increase in the caronic acid formation between experiments at 0 and 20 °C.

The particle fraction of each species can be expressed as particle-phase fraction (F_p), which is a proxy of volatility.[93] The F_p of caronic acid is calculated from the normalised signals in the gas and the particle phases according to eqn (1) at each time point.

$$F_p(\text{caronic acid}) = \frac{C_{10}H_{16}O_{3,\text{particle}}}{C_{10}H_{16}O_{3,\text{gas}} + C_{10}H_{16}O_{3,\text{particle}}} \quad (1)$$

The average F_p values of caronic acid from experiments 0A and 20B are 0.48 and 0.26, respectively, showing a decrease as the temperature increase. The F_p values of caronic acid from the chamber study of Δ^3-carene ozonolysis are close to other reports of observed F_p values of pinonic acid (0.1–0.3).[94,95] The increase in F_p with decreasing temperature is expected as condensation of organics is enhanced with decreasing temperature.[63,89,96,97] It is also in line with previous research for semi-volatile oxidation products from both ozonolysis of α-pinene[25,26] and Δ^3-carene.[34] Fig. S.11† shows the concentration of *cis*-3-caronic acid quantified with the offline analysis of experiment 20A. According to the ADCHAM model experiment 20B was performed with an increased VOC loading (14 ppb, Table 1 and Section 3.3), which will increase the resulting fraction of products compared to experiment 20A (10 ppb, Table 1 and Section 3.3). In agreement with the FIGAERO data, the concentration of *cis*-3-caronic acid measured by offline analysis in the particle phase at 20 °C exceeds that of *cis*-3-caronic acid in the particle phase at 0 °C until ~120 min. At 150 minutes, the concentration of *cis*-3-caronic acid is higher at 0 °C than at 20 °C. A more extensive investigation of the partitioning of caronic acid and other ozonolysis products produced in the two experiments will be discussed in a separate paper.

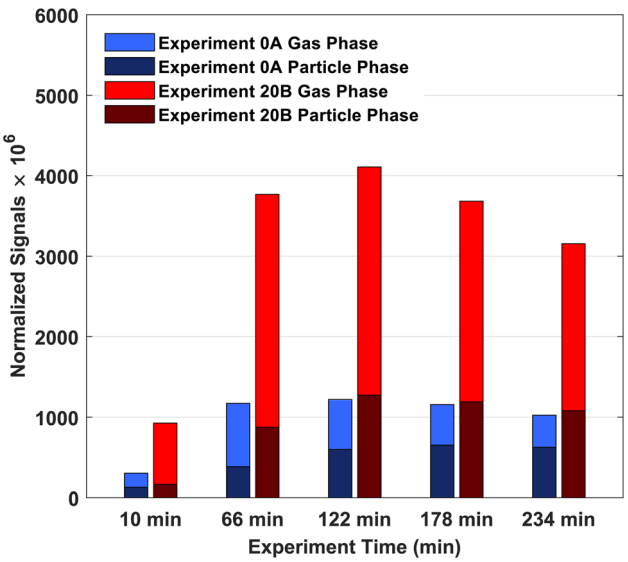

Fig. 7 Normalised signals of ozonolysis product ($C_{10}H_{16}O_3$) of Δ^3-carene in experiments 0A and 20B at experiment times 0–10 min, 56–66 min, 112–122 min, 168–178 min, and 224–234 min. Signals are normalised by reagent I^- signal and multiplied with 10^6.

4 Conclusion

In the ACCEPTO campaign, multiple state-of-the-art analysis methods for both gas phase and particle phase species were applied to investigate the formation and composition of SOA from Δ^3-carene.

The SOA formation from ozonolysis of Δ^3-carene does not show a strong effect of temperature in particle number concentration or SOA yields, which is in agreement with previous research on the SOA formation from Δ^3-carene. This is a surprising finding as the formation of SOA from the structurally similar monoterpene α-pinene exhibits increasing particle number concentrations and particle mass concentrations with decreasing temperature.

A slight temperature dependence is, however, observed in the composition of the particle phase, where the mass fractions of the tentatively identified carboxylic acids *cis*-3-caric acid, *cis*-3-caronic acid, and OH–caronic acid show an increase over time at 0 °C and a decrease over time at 20 °C. In the gas phase, an increase in the signal intensity from caronic acid is observed with increasing temperature. Likewise, the signal intensity from caronic acid in the particle phase increases slightly with increasing temperature. The formation of the HOM monomers, $C_{10}H_{14}O_9$ and $C_{10}H_{16}O_9$, are enhanced with increasing temperature in agreement with previous observations for ozonolysis of α-pinene.

A very large increase in the particle number concentration and the nucleation rate is observed with increasing RH (80% *vs.* 0%), while the particle mass concentration is not affected suggesting that the nucleation is driven by inorganics in these experiments.

The modelled SOA mass concentrations are within the experimental uncertainties of all experiments and in general, agree well with the experimental observations.

In conclusion, the experimental results indicate that the SOA formation from Δ^3-carene is not as dependent on temperature as the SOA formation from α-pinene, but that there is an effect of the presence of water vapour. However, the ADCHAM model simulations of idealised dry atmospheric simulation chamber conditions, *i.e.* without wall losses or chamber dilution effects, show a factor of 2 increase in the SOA mass yields when the temperature decreases from 20 to 0 °C. Thus, further studies are needed to explain the mechanisms of the temperature and water-dependent chemistry for Δ^3-carene ozonolysis and to quantify the corresponding SOA mass yield dependencies.

Data availability

The data is available upon request. All data is available from the ATMO-ACCESS Database of Atmospheric Simulation Chamber

Studies at the following DOIs: https://doi.org/10.25326/TBWC-R133, https://doi.org/10.25326/62Y1-3K47, https://doi.org/10.25326/DT8P-XF52, https://doi.org/10.25326/D1A9-G032, https://doi.org/10.25326/V4X9-EX29, https://doi.org/10.25326/6XQN-5852, https://doi.org/10.25326/MWVJ-TT47, and https://doi.org/10.25326/BF7F-F767.

Author contributions

Conceptualisation: DT, EMI, HBP, PR, ME, MH, MG, and MB. Investigation: DT, EMI, JTS, YL, LL, and MP. Formal analysis: DT, EMI, JTS, YL, LL, and MP. ADCHAM model calculations: PR. Visualisation: DT, EMI, JTS, YL, LL, and PR. DT, EMI, JTS, YL, LL, MP, PR, HBP, MH, ME, MB, and MG took part in the scientific discussion. Writing – original draft: DT, EMI, JTS with large contributions from YL, LL, and PR. Writing – review & editing: all authors. Data curation: DT, EMI, JTS, MB, MG.

Conflicts of interest

The authors declare no conflicts of interest.

Acknowledgements

The ACCEPTO campaign is part of a project that is supported by the European Commission under the Horizon 2020 – Research and Innovation Framework Programme, through the ATMO-ACCESS Integrating Activity under grant agreement no. 101008004. We thank the Independent Research Fund Denmark (0136-00345B, 8021-00355B), the Carlsberg Foundation, Danish Agency for Higher Education and Science (ACTRIS-DK, 5072-00032B), Aarhus University, the Danish National Research Foundation through the Center of Excellence for Chemistry of Clouds (Grant Agreement No. DNRF172), the Research Council of Finland, the Swedish Research Council (Formas project no. 2018-01745-COBACCA), the Swedish Research Council VR (project no. 2019-05006) and the Crafoord Foundation (project no. 20210969) for their financial support. We thank laboratory manager Mads Mørk Jensen for his assistance in the laboratory. We thank Eva R. Kjærgaard and Þuríður Nótt Björgvinsdottír for their help during the campaign. We thank the workshops at the Department of Chemistry, Aarhus University for technical support.

References

1 J. L. Jimenez, M. R. Canagaratna, N. M. Donahue, A. S. H. Prevot, Q. Zhang, J. H. Kroll and *et al.*, Evolution of Organic Aerosols in the Atmosphere, *Science*, 2009, **326**, 1525–1529.

2 V. Masson-Delmotte, P. Zhai, A. Pirani, S. Connors, C. Péan and S. Berger, *et al.*, in *Climate Change 2021: the Physical Science Basis. Contribution of Working Group I to the Sixth Assessment Report of the Intergovernmental Panel on Climate Change*, Cambridge University Press, 2021.

3 M. Hallquist, J. C. Wenger, U. Baltensperger, Y. Rudich, D. Simpson, M. Claeys and *et al.*, The formation, properties and impact of secondary organic aerosol: current and emerging issues, *Atmos. Chem. Phys.*, 2009, **9**, 5155–5236.

4 M. Shiraiwa, K. Ueda, A. Pozzer, G. Lammel, C. J. Kampf, A. Fushimi and *et al.*, Aerosol Health Effects from Molecular to Global Scales, *Environ. Sci. Technol.*, 2017, **51**, 13545–13567.

5 M. Kanakidou, J. H. Seinfeld, S. N. Pandis, I. Barnes, F. J. Dentener, M. C. Facchini and *et al.*, Organic aerosol and global climate modelling: a review, *Atmos. Chem. Phys.*, 2005, **5**, 1053–1123.

6 A. Guenther, C. N. Hewitt, D. Erickson, R. Fall, C. Geron, T. Graedel and *et al.*, A global model of natural volatile organic compound emissions, *J. Geophys. Res.: Atmos.*, 1995, **100**, 8873–8892.

7 K. Sindelarova, C. Granier, I. Bouarar, A. Guenther, S. Tilmes, T. Stavrakou, J.-F. Müller, U. Kuhn, P. Stefani and W. Knorr, Global data set of biogenic VOC emissions calculated by the MEGAN model over the last 30 years, *Atmos. Chem. Phys.*, 2014, **14**, 9317–9341.

8 J. Bäck, J. Aalto, M. Henriksson, H. Hakola, Q. He and M. Boy, Chemodiversity of a Scots pine stand and implications for terpene air concentrations, *Biogeosciences*, 2012, **9**, 689–702.

9 J. L. Fry, D. C. Draper, K. J. Zarzana, P. Campuzano-Jost, D. A. Day, J. L. Jimenez and *et al.*, Observations of gas- and aerosol-phase organic nitrates at BEACHON-RoMBAS 2011, *Atmos. Chem. Phys.*, 2013, **13**, 8585–8605.

10 M. Ehn, J. A. Thornton, E. Kleist, M. Sipilä, H. Junninen, I. Pullinen and *et al.*, A large source of low-volatility secondary organic aerosol, *Nature*, 2014, **506**, 476–479.

11 J. D. Crounse, L. B. Nielsen, S. Jørgensen, H. G. Kjaergaard and P. O. Wennberg, Autoxidation of Organic Compounds in the Atmosphere, *J. Phys. Chem. Lett.*, 2013, **4**, 3513–3520.

12 F. Bianchi, T. Kurtén, M. Riva, C. Mohr, M. P. Rissanen, P. Roldin and *et al.*, Highly Oxygenated Organic Molecules (HOM) from Gas-Phase Autoxidation Involving Peroxy Radicals: A Key Contributor to Atmospheric Aerosol, *Chem. Rev.*, 2019, **119**, 3472–3509.

13 N. M. Donahue, J. H. Kroll, S. N. Pandis and A. L. Robinson, A two-dimensional volatility basis set – part 2: diagnostics of organic-aerosol evolution, *Atmos. Chem. Phys.*, 2012, **12**, 615–634.

14 F. Bianchi, J. Tröstl, H. Junninen, C. Frege, S. Henne, C. R. Hoyle and *et al.*, New particle formation in the free troposphere: a question of chemistry and timing, *Science*, 2016, **352**, 1109–1112.

15 U. Molteni, M. Simon, M. Heinritzi, C. R. Hoyle, A.-K. Bernhammer, F. Bianchi and *et al.*, Formation of Highly Oxygenated Organic Molecules from α-Pinene Ozonolysis: Chemical Characteristics, Mechanism, and Kinetic Model Development, *ACS Earth Space Chem.*, 2019, **3**, 873–883.

16 O. Peräkylä, T. Berndt, L. Franzon, G. Hasan, M. Meder, R. R. Valiev and *et al.*, Large Gas-Phase Source of Esters and Other Accretion Products in the Atmosphere, *J. Am. Chem. Soc.*, 2023, **145**, 7780–7790, PMID: 36995167.

17 T. Hoffmann, R. Bandur, U. Marggraf and M. Linscheid, Molecular composition of organic aerosols formed in the α-pinene/O_3 reaction: implications for new particle formation processes, *J. Geophys. Res.: Atmos.*, 1998, **103**, 25569–25578.

18 M. P. Tolocka, M. Jang, J. M. Ginter, F. J. Cox, R. M. Kamens and M. V. Johnston, Formation of Oligomers in Secondary Organic Aerosol, *Environ. Sci. Technol.*, 2004, **38**, 1428–1434.

19 F. Yasmeen, R. Szmigielski, R. Vermeylen, Y. Gómez-González, J. D. Surratt, A. W. H. Chan, J. H. Seinfeld, W. Maenhaut and M. Claeys, Mass spectrometric characterization of isomeric terpenoic acids from the oxidation of α-pinene, β-pinene, d-limonene, and Δ^3-carene in fine forest aerosol, *J. Mass Spectrom.*, 2011, **46**, 425–442.

20 K. Kristensen, K. L. Enggrob, S. M. King, D. R. Worton, S. M. Platt, R. Mortensen and *et al.*, Formation and occurrence of dimer esters of pinene oxidation products in atmospheric aerosols, *Atmos. Chem. Phys.*, 2013, **13**, 3763–3776.

21 K. Kristensen, T. Cui, H. Zhang, A. Gold, M. Glasius and J. D. Surratt, Dimers in α-pinene secondary organic aerosol: effect of hydroxyl radical, ozone, relative humidity and aerosol acidity, *Atmos. Chem. Phys.*, 2014, **14**, 4201–4218.

22 K. Kristensen, M. Bilde, P. P. Aalto, T. Petäjä and M. Glasius, Denuder/filter sampling of organic acids and organosulfates at urban and boreal forest sites: gas/particle distribution and possible sampling artifacts, *Atmos. Environ.*, 2016, **130**, 36–53.

23 K. Kristensen, Å. K. Watne, J. Hammes, A. Lutz, T. Petäjä, M. Hallquist, M. Bilde and M. Glasius, High-Molecular Weight Dimer Esters Are Major Products in Aerosols from α-Pinene Ozonolysis and the Boreal Forest, *Environ. Sci. Technol. Lett.*, 2016, **3**, 280–285.

24 C. Mohr, F. D. Lopez-Hilfiker, T. Yli-Juuti, A. Heitto, A. Lutz, M. Hallquist and *et al.*, Ambient observations of dimers from terpene oxidation in the gas phase: implications for new particle formation and growth, *Geophys. Res. Lett.*, 2017, **44**, 2958–2966.

25 K. Kristensen, L. N. Jensen, M. Glasius and M. Bilde, The effect of sub-zero temperature on the formation and composition of secondary organic aerosol from ozonolysis of alpha-pinene, *Environ. Sci.: Processes Impacts*, 2017, **19**, 1220–1234.

26 K. Kristensen, L. N. Jensen, L. L. J. Quéléver, S. Christiansen, B. Rosati, J. Elm and *et al.*, The Aarhus Chamber Campaign on Highly Oxygenated Organic Molecules and Aerosols (ACCHA): Particle Formation, Organic Acids, and Dimer Esters from α-Pinene Ozonolysis at Different Temperatures, *Atmos. Chem. Phys.*, 2020, **20**, 12549–12567.

27 G. Hasan, V.-T. Salo, R. R. Valiev, J. Kubečka and T. Kurtén, Comparing Reaction Routes for 3(RO···OR') Intermediates Formed in Peroxy Radical Self- and Cross-Reactions, *J. Phys. Chem. A*, 2020, **124**, 8305–8320.

28 V.-T. Salo, R. Valiev, S. Lehtola and T. Kurtén, Gas-Phase Peroxyl Radical Recombination Reactions: A Computational Study of Formation and Decomposition of Tetroxides, *J. Phys. Chem. A*, 2022, **126**, 4046–4056.

29 J. Hamilton, A. Lewis, J. Reynolds, L. Carpenter and A. Lubben, Investigating the composition of organic aerosol resulting from cyclohexene ozonolysis: low molecular weight and heterogeneous reaction products, *Atmos. Chem. Phys.*, 2006, **6**, 4973–4984.

30 L. Müller, M.-C. Reinnig, J. Warnke and T. Hoffmann, Unambiguous identification of esters as oligomers in secondary organic aerosol formed from cyclohexene and cyclohexene/α- pinene ozonolysis, *Atmos. Chem. Phys.*, 2008, **8**, 1423–1433.

31 S. Gao, N. L. Ng, M. Keywood, V. Varutbangkul, R. Bahreini, A. Nenes and *et al.*, Particle Phase Acidity and Oligomer Formation in Secondary Organic Aerosol, *Environ. Sci. Technol.*, 2004, **38**, 6582–6589.

32 Y. Zhao, M. Yao, Y. Wang, Z. Li, S. Wang, C. Li and H. Xiao, Acylperoxy Radicals as Key Intermediates in the Formation of Dimeric Compounds in α-Pinene Secondary Organic Aerosol, *Environ. Sci. Technol.*, 2022, **56**, 14249–14261, PMID: 36178682.

33 Y. Zhang, Y. Chen, Z. Lei, N. E. Olson, M. Riva, A. R. Koss and *et al.*, Joint Impacts of Acidity and Viscosity on the Formation of Secondary Organic Aerosol from Isoprene Epoxydiols (IEPOX) in Phase Separated Particles, *ACS Earth Space Chem.*, 2019, **3**, 2646–2658.

34 D. Thomsen, J. Elm, B. Rosati, J. T. Skønager, M. Bilde and M. Glasius, Large Discrepancy in the Formation of Secondary Organic Aerosols from Structurally Similar Monoterpenes, *ACS Earth Space Chem.*, 2021, **5**, 632–644.

35 D. Thomsen, L. D. Thomsen, E. M. Iversen, T. N. Björgvinsdóttir, S. F. Vinther, J. T. Skønager, T. Hoffmann, J. Elm, M. Bilde and M. Glasius, Ozonolysis of α-Pinene and Δ^3-Carene Mixtures: Formation of Dimers with Two Precursors, *Environ. Sci. Technol.*, 2022, **56**, 16643–16651.

36 M. Glasius, M. Lahaniati, A. Calogirou, D. Di Bella, N. R. Jensen, J. Hjorth, D. Kotzias and B. R. Larsen, Carboxylic Acids in Secondary Aerosols from Oxidation of Cyclic Monoterpenes by Ozone, *Environ. Sci. Technol.*, 2000, **34**, 1001–1010.

37 Y. Y. Zhang, L. Müller, R. Winterhalter, G. K. Moortgat, T. Hoffmann and U. Pöschl, Seasonal cycle and temperature dependence of pinene oxidation products, dicarboxylic acids and nitrophenols in fine and coarse air particulate matter, *Atmos. Chem. Phys.*, 2010, **10**, 7859–7873.

38 M. Glasius and A. H. Goldstein, Recent Discoveries and Future Challenges in Atmospheric Organic Chemistry, *Environ. Sci. Technol.*, 2016, **50**, 2754–2764.

39 J. Yu, D. R. Cocker III, R. J. Griffin, R. C. Flagan and J. H. Seinfeld, *J. Atmos. Chem.*, 1999, **34**, 207–258.

40 F. D. Lopez-Hilfiker, C. Mohr, M. Ehn, F. Rubach, E. Kleist, J. Wildt and *et al.*, A novel method for online analysis of gas and particle composition: description and evaluation of a Filter Inlet for Gases and AEROsols (FIGAERO), *Atmos. Meas. Tech.*, 2014, **7**, 983–1001.

41 T. Hoffmann, J. R. Odum, F. Bowman, D. Collins, D. Klockow, R. C. Flagan and J. H. Seinfeld, Formation of Organic Aerosols from the Oxidation of Biogenic Hydrocarbons, *J. Atmos. Chem.*, 1997, **26**, 189–222.

42 Å. M. Jonsson, M. Hallquist and E. Ljungström, Impact of Humidity on the Ozone Initiated Oxidation of Limonene, Δ^3-Carene, and α-Pinene, *Environ. Sci. Technol.*, 2006, **40**, 188–194, PMID: 16433350.

43 Å. M. Jonsson, M. Hallquist and E. Ljungström, The effect of temperature and water on secondary organic aerosol formation from ozonolysis of limonene, and Δ^3-carene and α- pinene, *Atmos. Chem. Phys.*, 2008, **8**, 6541–6549.

44 B. Witkowski and T. Gierczak, Early stage composition of SOA produced by α-pinene/ozone reaction: α-acyloxyhydroperoxy aldehydes and acidic dimers, *Atmos. Environ.*, 2014, **95**, 59–70.

45 L. L. J. Quéléver, K. Kristensen, L. Normann Jensen, B. Rosati, R. Teiwes, K. R. Daellenbach and *et al.*, Effect of temperature on the formation of highly oxygenated organic molecules (HOMs) from alpha-pinene ozonolysis, *Atmos. Chem. Phys.*, 2019, **19**, 7609–7625.

46 M. Simon, L. Dada, M. Heinritzi, W. Scholz, D. Stolzenburg, L. Fischer and *et al.*, Molecular understanding of new-particle formation from α-pinene between −50 and +25 °C, *Atmos. Chem. Phys.*, 2020, **20**, 9183–9207.

47 Q. Ye, M. Wang, V. Hofbauer, D. Stolzenburg, D. Chen, M. Schervish, A. Vogel, R. L. Mauldin, R. Baalbaki, S. Brilke and *et al.*, Molecular composition and volatility of nucleated particles from α-pinene oxidation between −50 °C and +25 °C, *Environ. Sci. Technol.*, 2019, **53**, 12357–12365.

48 L. Caudillo, B. Rörup, M. Heinritzi, G. Marie, M. Simon, A. C. Wagner and *et al.*, Chemical composition of nanoparticles from α-pinene nucleation and the influence of isoprene and relative humidity at low temperature, *Atmos. Chem. Phys.*, 2021, **21**, 17099–17114.

49 M. Surdu, H. Lamkaddam, D. S. Wang, D. M. Bell, M. Xiao, C. P. Lee and *et al.*, Molecular Understanding of the Enhancement in Organic Aerosol Mass at High Relative Humidity, *Environ. Sci. Technol.*, 2023, **57**, 2297–2309, PMID: 36716278.

50 E. L. D'Ambro, S. Schobesberger, C. J. Gaston, F. D. Lopez-Hilfiker, B. H. Lee, J. Liu and *et al.*, Chamber-based insights into the factors controlling epoxydiol (IEPOX) secondary organic aerosol (SOA) yield, composition, and volatility, *Atmos. Chem. Phys.*, 2019, **19**, 11253–11265.

51 D. A. Day, J. L. Fry, H. G. Kang, J. E. Krechmer, B. R. Ayres, N. I. Keehan and *et al.*, Secondary Organic Aerosol Mass Yields from NO_3 Oxidation of α-Pinene and Δ-Carene: Effect of RO_2 Radical Fate, *J. Phys. Chem. A*, 2022, **126**, 7309–7330.

52 M. Boy, D. Mogensen, S. Smolander, L. Zhou, T. Nieminen, P. Paasonen and *et al.*, Oxidation of SO_2 by stabilized Criegee intermediate (sCI) radicals as a crucial source for atmospheric sulfuric acid concentrations, *Atmos. Chem. Phys.*, 2013, **13**, 3865–3879.

53 B. Bonn and G. K. Moorgat, New particle formation during a- and b-pinene oxidation by O_3, OH and NO_3, and the influence of water vapour: particle size distribution studies, *Atmos. Chem. Phys.*, 2002, **2**, 183–196.

54 R. Tillmann, M. Hallquist, Å. M. Jonsson, A. Kiendler-Scharr, H. Saathoff, Y. Iinuma and T. F. Mentel, Influence of relative humidity and temperature on the production of pinonaldehyde and OH radicals from the ozonolysis of α-pinene, *Atmos. Chem. Phys.*, 2010, **10**, 7057–7072.

55 X. Li, S. Chee, J. Hao, J. P. D. Abbatt, J. Jiang and J. N. Smith, Relative humidity effect on the formation of highly oxidized molecules and new particles during monoterpene oxidation, *Atmos. Chem. Phys.*, 2019, **19**, 1555–1570.

56 M. Sipilä, T. Berndt, T. Petäjä, D. Brus, J. Vanhanen, F. Stratmann and *et al.*, The Role of Sulfuric Acid in Atmospheric Nucleation, *Science*, 2010, **327**, 1243–1246.

57 J. Vanhanen, J. Mikkilä, K. Lehtipalo, M. Sipilä, H. E. Manninen, E. Siivola, T. Petäjä and M. Kulmala, Particle Size Magnifier for Nano-CN Detection, *Aerosol Sci. Technol.*, 2011, **45**, 533–542.

58 P. F. DeCarlo, J. R. Kimmel, A. Trimborn, M. J. Northway, J. T. Jayne, A. C. Aiken and *et al.*, Field-Deployable, High-Resolution, Time-of-Flight Aerosol Mass Spectrometer, *Anal. Chem.*, 2006, **78**, 8281–8289.

59 A. E. Fernandez, G. S. Lewis and S. V. Hering, Design and Laboratory Evaluation of a Sequential Spot Sampler for Time-Resolved Measurement of Airborne Particle Composition, *Aerosol Sci. Technol.*, 2014, **48**, 655–663.

60 A. Eiguren Fernandez, G. S. Lewis, S. R. Spielman and S. V. Hering, Time-resolved Characterization of Particle Associated Polycyclic Aromatic Hydrocarbons using a Newly-developed Sequential Spot Sampler with Automated Extraction and Analysis, *Atmos. Environ.*, 2014, **96**, 125–134.

61 H. Junninen, M. Ehn, T. Petäjä, L. Luosujärvi, T. Kotiaho, R. Kostiainen and *et al.*, A highresolution mass spectrometer to measure atmospheric ion composition, *Atmos. Meas. Tech.*, 2010, **3**, 1039–1053.

62 T. Jokinen, M. Sipilä, H. Junninen, M. Ehn, G. Lönn, J. Hakala, T. Petäjä, R. L. Mauldin III, M. Kulmala and D. R. Worsnop, Atmospheric sulphuric acid and neutral cluster measurements using CI-APi-TOF, *Atmos. Chem. Phys.*, 2012, **12**, 4117–4125.

63 R. K. Pathak, C. O. Stanier, N. M. Donahue and S. N. Pandis, Ozonolysis of α-pinene at atmospherically relevant concentrations: temperature dependence of aerosol mass fractions (yields), *J. Geophys. Res.: Atmos.*, 2007, **112**, D03201.

64 J. R. Odum, T. Hoffmann, F. Bowman, D. Collins, R. C. Flagan and J. H. Seinfeld, Gas/Particle Partitioning and Secondary Organic Aerosol Yields, *Environ. Sci. Technol.*, 1996, **30**, 2580–2585.

65 M. Tomicic, M. Bødker Enghoff and H. Svensmark, Experimental study of H_2SO_4 aerosol nucleation at high ionization levels, *Atmos. Chem. Phys.*, 2018, **18**, 5921–5930.

66 M. Kulmala, T. Petäjä, T. Nieminen, M. Sipilä, H. E. Manninen, K. Lehtipalo and *et al.*, Measurement of the nucleation of atmospheric aerosol particles, *Nat. Protoc.*, 2012, **7**, 1651–1667.

67 K. E. J. Lehtinen and M. Kulmala, A model for particle formation and growth in the atmosphere with molecular resolution in size, *Atmos. Chem. Phys.*, 2003, **3**, 251–257.
68 X. Su, X. Yan and C.-L. Tsai, Linear regression, *Wiley Interdiscip. Rev. Comput. Stat.*, 2012, **4**, 275–294.
69 M. Claeys, Y. Iinuma, R. Szmigielski, J. D. Surratt, F. Blockhuys, C. Van Alsenoy and *et al.*, Terpenylic Acid and Related Compounds from the Oxidation of α-Pinene: Implications for New Particle Formation and Growth above Forests, *Environ. Sci. Technol.*, 2009, **43**, 6976–6982.
70 A. Kahnt, R. Vermeylen, Y. Iinuma, M. Safi Shalamzari, W. Maenhaut and M. Claeys, Highmolecular-weight esters in α-pinene ozonolysis secondary organic aerosol: structural characterization and mechanistic proposal for their formation from highly oxygenated molecules, *Atmos. Chem. Phys.*, 2018, **18**, 8453–8467.
71 H. Junninen, PhD thesis, Faculty of Science, University of Helsinki, 2014.
72 P. Roldin, A. C. Eriksson, E. Z. Nordin, E. Hermansson, D. Mogensen, A. Rusanen and *et al.*, Modelling non-equilibrium secondary organic aerosol formation and evaporation with the aerosol dynamics, gas- and particle-phase chemistry kinetic multilayer model ADCHAM, *Atmos. Chem. Phys.*, 2014, **14**, 7953–7993.
73 S. M. Saunders, M. E. Jenkin, R. Derwent and M. Pilling, Protocol for the development of the master chemical mechanism, MCM v3 (part A): tropospheric degradation of nonaromatic volatile organic compounds, *Atmos. Chem. Phys.*, 2003, **3**, 161–180.
74 M. Jenkin, J. Young and A. Rickard, The MCM v3. 3.1 degradation scheme for isoprene, *Atmos. Chem. Phys.*, 2015, **15**, 11433–11459.
75 P. Roldin, M. Ehn, T. Kurtén, T. Olenius, M. P. Rissanen, N. Sarnela and *et al.*, The role of highly oxygenated organic molecules in the Boreal aerosol-cloud-climate system, *Nat. Commun.*, 2019, **10**, 1–15.
76 W. Nie, C. Yan, L. Yang, P. Roldin, Y. Liu, A. L. Vogel, *et al.*, NO at low concentration can enhance the formation of highly oxygenated biogenic molecules in the atmosphere, *Nat. Commun.*, 2023, **14**, 3347.
77 L. Hantschke, A. Novelli, B. Bohn, C. Cho, D. Reimer, F. Rohrer, R. Tillmann, M. Glowania, A. Hofzumahaus, A. Kiendler-Scharr and *et al.*, Atmospheric photooxidation and ozonolysis of Δ 3-carene and 3-caronaldehyde: rate constants and product yields, *Atmos. Chem. Phys.*, 2021, **21**, 12665–12685.
78 T. J. Dillon, K. Dulitz, C. Groß and J. N. Crowley, Temperature-dependent rate coefficients for the reactions of the hydroxyl radical with the atmospheric biogenics isoprene, alphapinene and delta-3-carene, *Atmos. Chem. Phys.*, 2017, **17**, 15137–15150.
79 L. Wang, Y. Liu and L. Wang, Ozonolysis of 3-carene in the atmosphere. Formation mechanism of hydroxyl radical and secondary ozonides, *Phys. Chem. Chem. Phys.*, 2019, **21**, 8081–8091.
80 J. Kirkby, J. Duplissy, K. Sengupta, C. Frege, H. Gordon, C. Williamson and *et al.*, Ion-induced nucleation of pure biogenic particles, *Nature*, 2016, **533**, 521–526.
81 E. M. Dunne, H. Gordon, A. Kürten, J. Almeida, J. Duplissy, C. Williamson and *et al.*, Global atmospheric particle formation from CERN CLOUD measurements, *Science*, 2016, **354**, 1119–1124.
82 J. Almeida, S. Schobesberger, A. Kürten, I. K. Ortega, O. Kupiainen-Määttä, A. P. Praplan and *et al.*, Molecular understanding of sulphuric acid–amine particle nucleation in the atmosphere, *Nature*, 2013, **502**, 359–363.
83 H. Henschel, J. C. A. Navarro, T. Yli-Juuti, O. Kupiainen-Määttä, T. Olenius, I. K. Ortega, S. L. Clegg, T. Kurtén, I. Riipinen and H. Vehkamäki, Hydration of Atmospherically Relevant Molecular Clusters: Computational Chemistry and Classical Thermodynamics, *J. Phys. Chem. A*, 2014, **118**, 2599–2611, PMID: 24678924.
84 F. R. Rasmussen, J. Kubečka, V. Besel, H. Vehkamäki, K. V. Mikkelsen, M. Bilde and J. Elm, Hydration of Atmospheric Molecular Clusters III: Procedure for Efficient Free Energy Surface Exploration of Large Hydrated Clusters, *J. Phys. Chem. A*, 2020, **124**, 5253–5261, PMID: 32463668.
85 O. Horie, P. Neeb and G. K. Moortgat, Ozonolysis of *trans*- and *cis*-2-butenes in low parts-per-million concentration ranges, *Int. J. Chem. Kinet.*, 1994, **26**, 1075–1094.
86 O. Horie, P. Neeb, S. Limbach and G. K. Moortgat, Formation of formic acid and organic peroxides in the ozonolysis of ethene with added water vapour, *Geophys. Res. Lett.*, 1994, **21**, 1523–1526.
87 C. L. Heald, J. H. Kroll, J. L. Jimenez, K. S. Docherty, P. F. DeCarlo, A. C. Aiken, Q. Chen, S. T. Martin, D. K. Farmer and P. Artaxo, A simplified description of the evolution of organic aerosol composition in the atmosphere, *Geophys. Res. Lett.*, 2010, **37**, L08803.
88 Y. Ma, T. R. Willcox, A. T. Russell and G. Marston, Pinic and pinonic acid formation in the reaction of ozone with α-pinene, *Chem. Commun.*, 2007, 1328–1330.
89 H. Saathoff, K.-H. Naumann, O. Möhler, Å. M. Jonsson, M. Hallquist, A. Kiendler-Scharr, T. F. Mentel, R. Tillmann and U. Schurath, Temperature dependence of yields of secondary organic aerosols from the ozonolysis of α-pinene and limonene, *Atmos. Chem. Phys.*, 2009, **9**, 1551–1577.
90 T. Jokinen, T. Berndt, R. Makkonen, V.-M. Kerminen, H. Junninen, P. Paasonen, F. Stratmann, H. Herrmann, A. B. Guenther, D. R. Worsnop and *et al.*, Production of extremely low volatile organic compounds from biogenic emissions: measured yields and atmospheric implications, *Proc. Natl. Acad. Sci. U. S. A.*, 2015, **112**, 7123–7128.
91 M. Ehn, T. Berndt, J. Wildt and T. Mentel, Highly Oxygenated Molecules from Atmospheric Autoxidation of Hydrocarbons: A Prominent Challenge for Chemical Kinetics Studies, *Int. J. Chem. Kinet.*, 2017, **49**, 821–831.
92 C. Frege, I. K. Ortega, M. P. Rissanen, A. P. Praplan, G. Steiner, M. Heinritzi, L. Ahonen, A. Amorim, A.-K. Bernhammer, F. Bianchi and *et al.*, Influence of temperature on the molecular composition of ions and

charged clusters during pure biogenic nucleation, *Atmos. Chem. Phys.*, 2018, **18**, 65–79.

93 N. M. Donahue, A. L. Robinson, C. O. Stanier and S. N. Pandis, Coupled Partitioning, Dilution, and Chemical Aging of Semivolatile Organics, *Environ. Sci. Technol.*, 2006, **40**, 2635–2643, PMID: 16683603.

94 A. Lutz, C. Mohr, M. Le Breton, F. D. Lopez-Hilfiker, M. Priestley, J. A. Thornton and M. Hallquist, Gas to particle partitioning of organic acids in the boreal atmosphere, *ACS Earth Space Chem.*, 2019, **3**, 1279–1287.

95 R. Yatavelli, H. Stark, S. Thompson, J. Kimmel, M. Cubison, D. Day, P. Campuzano-Jost, B. Palm, A. Hodzic, J. Thornton and *et al.*, Semicontinuous measurements of gas–particle partitioning of organic acids in a ponderosa pine forest using a MOVI-HRToF-CIMS, *Atmos. Chem. Phys.*, 2014, **14**, 1527–1546.

96 T. M. Svendby, M. Lazaridis and K. Tørseth, Temperature dependent secondary organic aerosol formation from terpenes and aromatics, *J. Atmos. Chem.*, 2008, **59**, 25–46.

97 B. Warren, R. L. Austin and D. R. Cocker, Temperature dependence of secondary organic aerosol, *Atmos. Environ.*, 2009, **43**, 3548–3555.